

# Non-touching nanoparticle diclusters bound by repulsive and attractive Casimir forces

Alejandro W. Rodriguez,<sup>1</sup> Alexander P. McCauley,<sup>1</sup> David Woolf,<sup>2</sup>  
Federico Capasso,<sup>2</sup> J. D. Joannopoulos,<sup>1</sup> and Steven G. Johnson<sup>3</sup>

<sup>1</sup>*Department of Physics, Massachusetts Institute of Technology, Cambridge, MA 02139*

<sup>2</sup>*Department of Applied Physics, Harvard University, Cambridge, MA 02139*

<sup>3</sup>*Department of Mathematics, Massachusetts Institute of Technology, Cambridge, MA 02139*

We present a scheme for obtaining stable Casimir suspension of dielectric nontouching objects immersed in a fluid, validated here in various geometries consisting of ethanol-separated dielectric spheres and semi-infinite slabs. Stability is induced by the dispersion properties of real dielectric (monolithic) materials. A consequence of this effect is the possibility of stable configurations (clusters) of compact objects, which we illustrate via a “molecular” two-sphere dicluster geometry consisting of two bound spheres levitated above a gold slab. Our calculations also reveal a strong interplay between material and geometric dispersion, and this is exemplified by the qualitatively different stability behavior observed in planar versus spherical geometries.

PACS numbers:

Electromagnetic fluctuations are the source of a macroscopic force between otherwise neutral objects known as the Casimir effect [1, 2, 3]. In most geometries involving vacuum-separated metallic or dielectric objects (with a separating plane), the force is attractive and decaying as a function of object separation, and may contribute to “stiction” in microelectromechanical systems [4]. A repulsive interaction would be desirable to combat stiction as well as for frictionless suspension and other applications. Repulsive Casimir forces occur in a variety of settings, including theoretical magnetic materials [5, 6, 7], fluid-separated dielectrics [8, 9], interleaved metallic geometries [10], and have also been suggested for composite metamaterials [11] (although repulsion with physical metamaterials has not yet been clearly demonstrated, as discussed below). In this letter, we demonstrate stable Casimir suspension of realistic dielectric/metallic objects immersed in a fluid. Unlike previous work [12, 13], this suspension does not involve one object enclosing another, but instead occurs between objects on opposite sides of an imaginary separating plane. This effect is a consequence of material dispersion, and is here validated in various experimentally accessible geometries consisting of ethanol-separated dielectric spheres and semi-infinite slabs. Furthermore, we show the possibility of achieving Casimir “molecular” clusters in which objects can form stable non-touching configurations in space—this is illustrated in a “diatomic” or “dicluster” geometry involving two dielectric (silicon/teflon) spheres of different radii bound into a non-touching pair and levitated above a gold slab. Finally, our calculations reveal interesting effects related to the interplay of geometric and material dispersion, in which stability responds to finite size in a way that is qualitatively different in planar or spherical geometries.

Casimir stability has been previously studied in at least four different contexts: first, in geometries involving mutually enclosed fluid-separated objects, in which

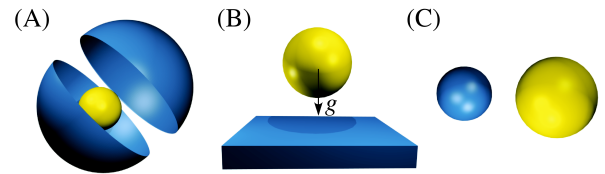


FIG. 1: Schematic schemes for stable suspension of fluid-separated objects, involving: (a) enclosed geometries; (b) gravity countering Casimir repulsion; and (c) material dispersion producing repulsive *and* attractive Casimir forces (here).

the inner object is repelled by the outer object [12, 13]; second, a slab–sphere geometry in which fluid-induced repulsion counteracts the force of gravity [14]; third, interleaved structures like the zipper geometry of [10], in which the surfaces of two complicated objects interleave so that their mutual attraction acts to separate the objects; and fourth, metamaterial proposals [11] that currently have no clear physical realization. The first two approaches (involving fluids) are illustrated by the schematics in Fig. 1(a–b). While all of these examples clearly demonstrate the possibility of Casimir stability, they leave something to be desired: they are limited to enclosed/complex geometries or require that stability lie only along a single direction (e.g. direction of gravity). It has been proposed that vacuum-separated chiral metamaterials may exhibit repulsive interactions and stable repulsive/attractive transitions [11], but the predicted repulsive forces arise only for small separations where the metamaterial approximation cannot be trusted, and recent exact calculations for the proposed structures indicate that they appear to be attractive [15]. Moreover, recent theoretical work has shown that vacuum-separated objects can never form stable configurations [16]. A less constrained and previously unexplored form of stability is one involving compact objects on either side of an imaginary separating plane, as illustrated in Fig. 1(c) for two

spheres: in this case (involving fluids), we will show that the objects form stable configurations that are independent of external forces, and seem more accessible to experiment, opening up new possibilities for the creation of multi-body clusters based on the Casimir force.

The Casimir force between two dielectric objects embedded in a fluid can become repulsive if their dielectric permittivities satisfy:

$$\varepsilon_1(i\xi) < \varepsilon_{\text{fluid}}(i\xi) < \varepsilon_2(i\xi), \quad (1)$$

over a sufficiently wide range of imaginary frequencies  $\xi$  [8]. The possibility of stable separations arises if the force transitions from repulsive at small separations (conceptually dominated by large- $\xi$  contributions) to attractive at large separations (conceptually dominated by small- $\xi$  contributions). A criterion for obtaining stability is therefore that Eq. (1) be violated at small  $\xi$ , and satisfied for  $\xi > \xi_c$ , with the transition occurring at some critical  $\xi_c \sim 2\pi c/\lambda_c$  roughly related to the lengthscale  $\lambda_c$  at which the repulsive/attractive transition occurs. This criterion is only heuristic, but helps guide our intuition. The real system is more complicated, as we shall see, because the sign of the force also depends on many other factors such as the relative strength of the contributions of different frequencies (related to the strength of the  $\varepsilon$  contrast) as well as on finite-size effects.

After considering a number of possibilities, we have identified several material combinations that satisfy Eq. (1) for large  $\xi$  (small separations). Figure 2(top) plots the dielectric permittivity  $\varepsilon(i\xi)$  of various materials (Si, teflon, SiO<sub>2</sub>, and ethanol) satisfying Eq. (1) over some large range of  $\xi$ . In order to establish the existence of stable separations, we first compute the force between semi-infinite slabs separated by ethanol, using the Lifshitz formula [2]. Figure 2(bottom) plots the Casimir force between semi-infinite slabs for different material arrangements, normalized by the corresponding force between perfectly-metallic slabs. Our results show that both teflon–Si (yellow) and SiO<sub>2</sub>–Si exhibit stable equilibria at  $d_c \approx 120\text{nm}$  and  $d_c^{(s)} \approx 90\text{nm}$ , respectively. SiO<sub>2</sub>–Si exhibits a finite region of stability coming from the existence of an *unstable* equilibrium at a smaller  $d_c^{(u)} \approx 29\text{nm}$ , a consequence of its two dielectric crossings  $\xi_c^{(1)} \approx 2.6\,2\pi c/\mu\text{m}$  and  $\xi_c^{(2)} \approx 26.4\,2\pi c/\mu\text{m}$  labelled in Fig. 2(top). As mentioned above, this prescription for obtaining stability is only heuristic: for example, the force between teflon–SiO<sub>2</sub> slabs is always attractive, even though their permittivities satisfy Eq. (1) at large  $\xi$ . In that case, while there is a crossing of the form of Eq. (1) at  $\xi_c^{(2)}$ , the repulsive contributions coming from  $\xi > \xi_c^{(2)}$  are overwhelmed by the attractive contributions coming from  $\xi < \xi_c^{(2)}$ , since SiO<sub>2</sub> and teflon become transparent at relatively small  $\xi$ . Thus, the repulsive region of the frequency spectrum merely *reduces* the attractive force

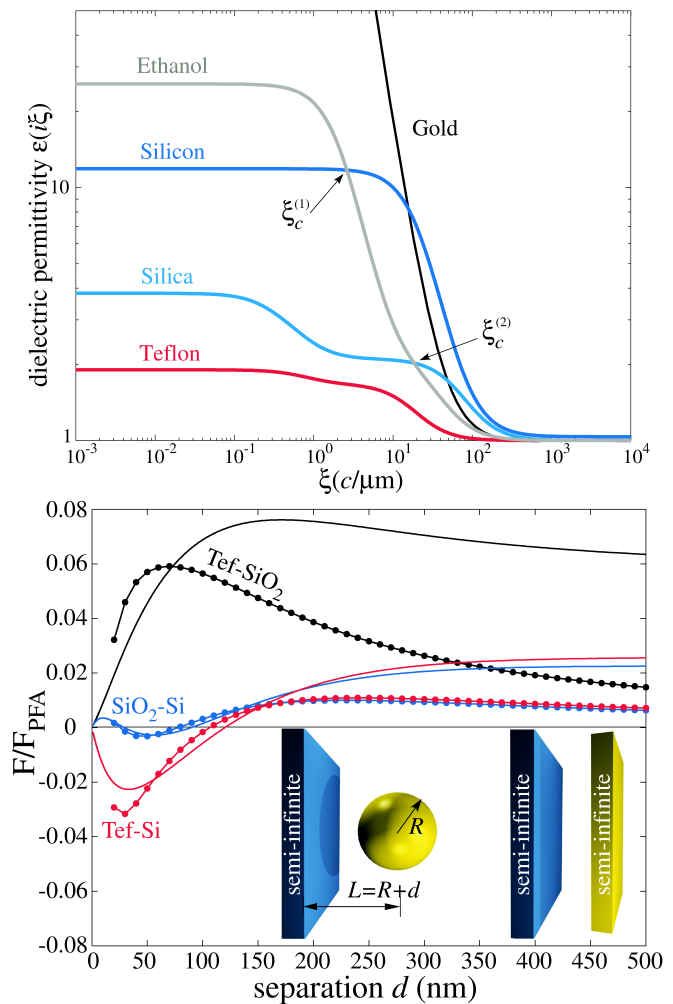


FIG. 2: (top): Plot of the dielectric permittivity  $\varepsilon(i\xi)$  of various materials evaluated at imaginary frequency  $\xi$  (in units of  $2\pi c/\mu\text{m}$ ). (Bottom:) Casimir force between a semi-infinite slab and a sphere (dots) or semi-finite slab (lines), normalized by the corresponding perfect-metal PFA force  $F_{\text{PFA}} = \hbar c \pi^3 / 720 d^3$  (slab-sphere) or  $F_{\text{PFA}} = \hbar c \pi^2 / 240 d^4$  (slab-slab). The force is plotted for various material configurations, explained in the text.

between the objects at small separations.

The existence of stable separations for semi-infinite slabs is promising, especially because this occurs in the 100nm range where Casimir forces are easily observable, leading us to investigate whether similar phenomena occur for finite-size objects: finite-thickness slabs, slab–sphere, and sphere–sphere configurations. For slab–sphere and sphere–sphere geometries, rapid exact calculations are performed using the spherical-harmonic scattering formulation of [17, 18], which converges exponentially fast (we only required spherical harmonics up to order  $\ell = 20$  to obtain better than 1% accuracy at relevant separations). Intuitively, one might expect the finite size or thickness of an object to suppress the contributions from small  $\xi$  (large “wavelengths”), and therefore to

change (or eliminate) the separation at which the repulsive/attractive transition occurs. Here, where attraction comes from small- $\xi$  contributions, one might expect the finite size to decrease the attractive contributions and therefore increase the equilibrium separation  $d_c$ .

Figure 2(bottom) plots the force between a sphere of radius  $R = 200\text{nm}$  and a semi-infinite slab for different material arrangements, normalized by the corresponding perfect-metal proximity-force approximation (PFA) force. (When referring to a geometry consisting of a semi-infinite  $\alpha$  and finite  $\beta$  object, we shall denote the combination by  $\alpha$ - $\beta$ . For example, when referring to the force between a semi-infinite teflon slab and a finite  $\text{SiO}_2$  sphere, we will use the notation Tef-SiO<sub>2</sub>.) The results in this slab-sphere geometry look qualitatively similar to those in the slab-slab structure. In particular, both Si-Tef and Si-SiO<sub>2</sub> exhibit stable equilibria at  $d_c \approx 105\text{nm}$  and  $d_c \approx 78\text{nm}$ , respectively, roughly  $15\text{nm}$  smaller than the  $d_c$  in the slab-slab case.

The fact that  $d_c$  is smaller in the slab-sphere case than for semi-infinite slabs was initially unexpected since it contradicts the intuition described above. However when we plot  $d_c$  for the various materials (solid dotted lines) as a function of  $R \in (0, 350)\text{nm}$  in Fig. 3, we indeed observe the expected behavior: as  $R$  decreases,  $d_c$  increases, asymptoting to a constant at  $R = 0$  that corresponds to the Casimir-Polder force between a spherical nanoparticle and a slab [17]. Similar increases in  $d_c$  as thickness  $t$  is decreased are observed in *some* of the finite-slab geometries (solid lines) in Fig. 3, at least in all of the configurations where the thickness of the silicon is varied. In the  $t \rightarrow \infty$  limit for the slab-slab case, the semi-infinite result is recovered. For the slab-sphere case with  $R \rightarrow \infty$ , the asymptotic  $d_c$  occurs for a smaller separation than for semi-infinite slabs: in this limit, where PFA is valid, the curvature of the spheres yields an average separation that is larger than  $d_c$ .

An interesting question is to what extent one may tailor object geometries in order to change the qualitative features of the force, e.g. its sign. With this question in mind, the dashed lines in Fig. 3 shows  $d_c$  for slab-slab geometries in which the two solid materials have been exchanged so that the semi-infinite slab is instead silicon. Apparently, changing which slab is finite qualitatively reverses the dependence on  $d_c$  in some cases: for Si-Au and Si-SiO<sub>2</sub> slabs, the equilibrium separation  $d_c$  *decreases* with decreasing thickness  $t$ , corresponding to an *increased* attractive force despite the fact that the attractive contributions arise from small  $\xi$  (which are intuitively cut off by the finite thickness). This reversal, however, does not happen in all cases: it does not occur for the Si-Tef slab-slab geometry or for *any* of the slab-sphere geometries (and we do not plot  $d_c$  in these reversed cases because the results are very similar to the original results). Evidently, the finite *lateral* size of the spheres has a dramatic qualitative interaction with the

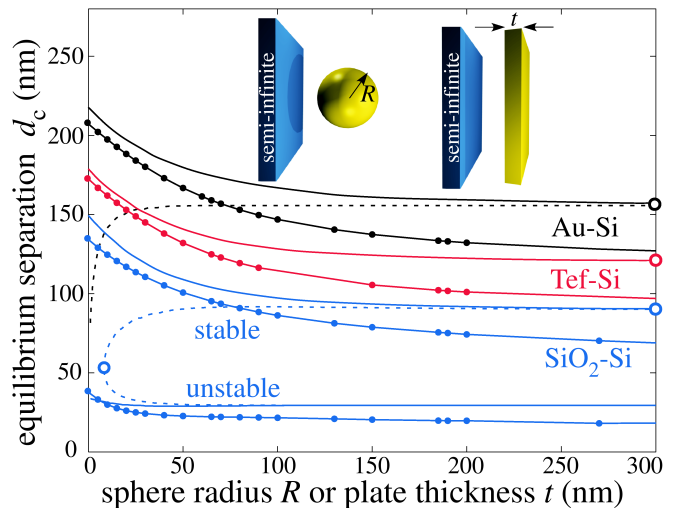


FIG. 3: Equilibrium separation  $d_c$  vs. sphere-radius ( $R$ ) or slab-thickness ( $t$ ) for various slab-sphere (dots) and slab-slab (lines) configurations. Dashed lines correspond to slab-slab geometries with materials swapped (semi-infinite silicon slab).

material dispersion. In future work, we plan to investigate this interesting interplay between material and geometric dispersion, in addition to the finite-size behavior exhibited by the finite gold [19] and SiO<sub>2</sub> slabs.

Another feature worth noting in Fig. 3 also stems from the anomalous response of the Si-SiO<sub>2</sub> slab-slab geometry to changes in the SiO<sub>2</sub> thickness  $t$ : the stable  $d_c^{(s)}$  and unstable  $d_c^{(u)}$  equilibria “collide” at a critical radius  $R_c$ , below which the force is purely attractive at all separations. Technically,  $R_c$  is the *tipping point* of a saddle-point bifurcation and the disappearance of both equilibria is an example of a fold catastrophe [20].

In what follows, we illustrate an interesting corollary of this type of stability: the possibility of obtaining stable noncontact configurations of compact objects at a nonzero separation. In particular, we calculate the Casimir force in a nanoparticle-dicluster system consisting of teflon and silicon spheres, of different radii  $R_T$  and  $R_S$ , respectively, immersed in ethanol. The force  $F_{SS}$  between the spheres is plotted in Fig. 4(bottom) for different sets of radii  $R_S = \{99.69, 293.67, 368.39\}\text{nm}$  and  $R_T = \{262.09, 32.67, 176.64\}\text{nm}$ , respectively. This choice of the radii was motivated by one possible experimental configuration, in which the pair of spheres are also levitated above a planar slab: in this geometry, discussed below, the sphere radii are chosen so that both spheres are suspended at the same height above the slab. With this choice of materials, the spheres are again attractive at large separations and repulsive for small separations, leading to a stable (orientation-independent) surface-surface separation in the  $100$ – $150\text{nm}$  range.

To make such a dicluster pair easier to observe in experiments, one could simultaneously suspend them at a

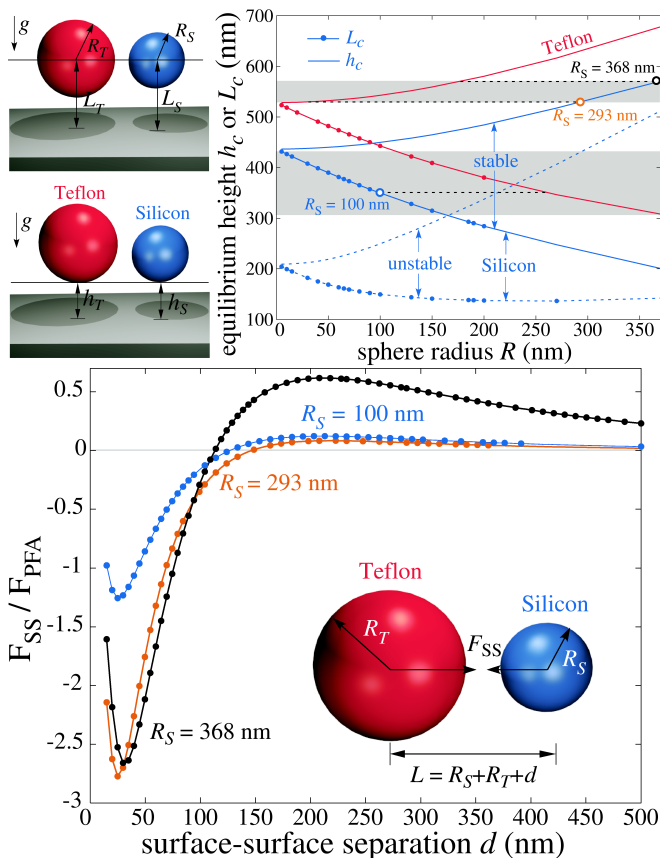


FIG. 4: (Top:) Plot of the stable equilibrium center–surface ( $L_c$ ) and surface–surface ( $h_c$ ) separation between either a teflon (yellow) or silicon (blue) sphere and a semi-infinite gold slab (depicted schematically on the left inset), as a function of sphere radius  $R$ . The black lines also show the presence of an unstable equilibrium in the silicon-sphere case. (Bottom:) Plot of the force  $F_{SS}$  between two teflon/silicon spheres of radii  $R_S/R_T$ , showing the existence of a stable equilibrium.

known distance above a planar substrate, using the interplay between the repulsive Casimir force and gravity to create stable levitation. For simplicity, we investigate this possibility within the additive approximation: the slab–sphere and sphere–sphere interactions are considered independently. Because Casimir forces are not additive, the presence of the slab will change the stable separation of the spheres (and vice versa for the stable height of the spheres). However, this approximation forms a useful starting point for the design of such an experiment and should even be accurate in the limit where the sphere diameter is much larger than the stable surface–surface separations (here, most of the diameters are at least twice the stable separations). Figure 4(top) shows a plot of the equilibrium surface–surface ( $h_c$ ) and center–surface ( $L_c = h_c + R$ ) separations of the teflon (yellow) and silicon (blue) spheres suspended above a semi-infinite gold slab, as a function of sphere radius  $R$ . As shown by the figure, decreasing  $R$  acts to increase  $h_c$  and decrease

$L_c$ . The decrease in  $h_c$  occurs much more rapidly than in Fig. 3 due to the fact that, in addition to geometric dispersion, the force of gravity scales as the mass  $\rho V$  of a sphere (where the density  $\rho \approx \{2330, 2200, 789\}$  kg/m<sup>3</sup>, for {Si, teflon, ethanol}, respectively). The center–center separation  $L_c = h_c + R$  increases with  $R$  because  $\partial h_c / \partial R > -1$ . In addition to a stable equilibrium  $h_c$ , Au–Si exhibits an unstable equilibrium at smaller  $d_c$  due to the transition to an attractive Casimir force for small separations; if the sphere were ever pushed below the unstable equilibrium point, it would continue downward and adhere to the slab. This would be a concern for experiments if fluctuations in the sphere height could push it below the unstable equilibrium, but as seen from Fig. 4 the distance between the stable and unstable equilibria is over 200nm for  $R < 50$ nm nanoparticles.

The gray areas in Fig. 4(top) depict regions in which the  $L_c$  or  $h_c$  of the two spheres can be made equal by an appropriate choice of radii, as shown schematically in Fig. 4(top-left). This determines the stable configuration of the two-sphere dicluster when they are brought together above the surface; the three dashed horizontal lines in Fig. 4(top) correspond to the radii used for the force calculation in Fig. 4(bottom).

We are grateful to Jeremy Munday at Caltech and Jamal S. Rahi at MIT for useful discussions. This work was supported by the Army Research Office through the ISN under Contract No. W911NF-07-D-0004, and by US DOE Grant No. DE-FG02-97ER25308 (AWR).

- 
- [1] H. B. G. Casimir, Proc. K. Ned. Akad. Wet. **51**, 793 (1948).
  - [2] E. M. Lifshitz and L. P. Pitaevskii, *Statistical Physics: Part 2* (Pergamon, Oxford, 1980).
  - [3] K. A. Milton, Journal of Physics A: Mathematical and General **37**, R209 (2004).
  - [4] H. B. Chan et al., Science **291**, 1941 (2001).
  - [5] T. H. Boyer, Phys. Rev. A **9**, 2078 (1974).
  - [6] O. Kenneth, I. Klich, A. Mann, and M. Revzen, Phys. Rev. Lett. **89**, 033001 (2002).
  - [7] F. S. S. Rosa, D. A. R. Dalvit, and P. Milonni, Phys. Rev. A **78**, 032117 (2008).
  - [8] I. E. Dzyaloshinskiĭ, E. M. Lifshitz, and L. P. Pitaevskii, Adv. Phys. **10**, 165 (1961).
  - [9] J. Munday, F. Capasso, and V. A. Parsegia, Nature **457**, 170 (2009).
  - [10] A. W. Rodriguez, J. D. Joannopoulos, and S. G. Johnson, Phys. Rev. A **79**, 013812 (2008).
  - [11] R. Zhao, J. Zhou, E. N. Economou, and C. M. Soukoulis, Phys. Rev. Lett. **103**, 103602 (2009).
  - [12] A. W. Rodriguez, J. Munday, D. Davlit, F. Capasso, J. D. Joannopoulos, and S. G. Johnson, Phys. Rev. Lett. **101**, 190404 (2008).
  - [13] S. J. Rahi and S. Zaheer, arXiv p. 0909.4510 (2009).
  - [14] A. P. McCauley et al., arXiv p. 0906.5170 (2009).
  - [15] A. P. McCauley et al., In preparation. (2009).

- [16] J. S. Rahi, M. Kardar, and T. Emig, arXiv p. 0911.5364 (2009).
- [17] S. J. Rahi, T. Emig, R. L. Jaffe, and M. Kardar, Phys. Rev. D **80**, 085021 (2009).
- [18] A. Lambrecht, P. A. Maia Neto, and S. Reynaud, New Journal of Physics **8** (2006).
- [19] A. Lambrecht, I. Pirozhenko, L. Duraffourg, and P. Andreucci, EPL **77**, 44006 (2006).
- [20] V. I. Arnold, *Catastrophe theory* (Berlin: Springer-Verlag, 1992), 3rd ed.